Nanoscale

COMMUNICATION

View Article Online
View Journal

Direct observation of hierarchical nucleation of martensite and size-dependent superelasticity in shape memory alloys†

Cite this: DOI: 10.1039/c3nr05258c

Received 2nd October 2013
Accepted 8th November 2013

DOI: 10.1039/c3nr05258c

www.rsc.org/nanoscale

Lifeng Liu,[a] Xiangdong Ding,*[a] Ju Li,*[bc] Turab Lookman[d] and Jun Sun*[a]

Martensitic transformation usually creates hierarchical internal structures beyond mere change of the atomic crystal structure. Multi-stage nucleation is thus required, where nucleation (level-1) of the underlying atomic crystal lattice does not have to be immediately followed by the nucleation of higher-order superstructures (level-2 and above), such as polysynthetic laths. Using *in situ* transmission electron microscopy (TEM), we directly observe the nucleation of the level-2 superstructure in a Cu–Al–Ni single crystal under compression, with critical super-nuclei size L_{2c} around 500 nm. When the sample size D decreases below L_{2c}, the superelasticity behavior changes from a flat stress plateau to a continuously rising stress–strain curve. Such size dependence definitely would impact the application of shape memory alloys in miniaturized MEMS/NEMS devices.

Shape memory alloys (SMAs) undergo phase transformation, *i.e.* change of the atomic crystal structure, under thermomechanical loading. This ability to undergo diffusionless shear-dominant transformations leads to technologically important properties of shape memory and superelasticity.[1–5] With the development of micro- and nano-electromechanical systems (MEMS/NEMS) exploiting "smart" materials,[6,7] it is of great interest to investigate superelasticity of small-volume SMAs, such as wires, pillars and particles.[8–14] Superelasticity is based on stress-induced martensitic transformation (SIMT) between austenite and martensite.[1,4] It is commonly believed that the onset of the stress plateau (τ_P) in the superelastic stress–strain curve upon loading is the critical stress at which martensite nucleates.[1,3,5,15] This, however, begs a fundamental clarification of what we mean by martensite: since we know temperature-driven martensitic transformation (TMT) often takes on hierarchical internal structures (*e.g.* Fig. 1(a)) like polysynthetic twin laths (level-2)[16,17] or even higher-level superstructures such as "herringbone",[18] beyond mere crystal lattice changes (level-1, conventionally used to define the phase transformation), is it

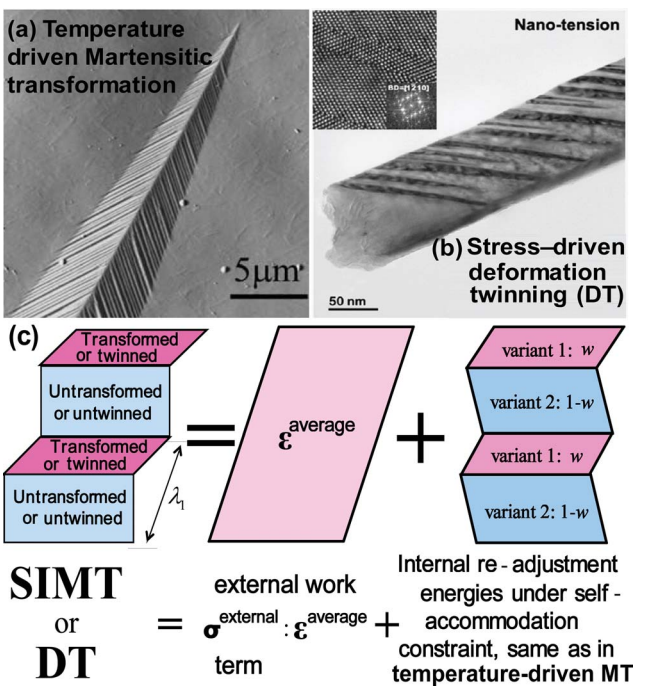

Fig. 1 Hierarchical superstructures in (a) temperature- and (b) stress-driven martensitic transformations ((a) TMT and (b) SIMT/DT). (a) is Cu–14.0Al–3.4Ni (wt.%) undergoing TMT (taken from ref. 21 with permission). (b) is small-volume Mg deformed in tension at room temperature (taken from ref. 20 with permission). (c) illustrates the conceptual equivalence between TMT and SIMT/DT in superstructure determination (λ_1 is the length scale of level-1 structure alternation and w is the volume fraction mixing weight of the two variants).

[a]State Key Laboratory for Mechanical Behavior of Materials, Xi'an Jiaotong University, Xi'an 710049, China. E-mail: dingxd@mail.xjtu.edu.cn; junsun@mail.xjtu.edu.cn

[b]Center for Advancing Materials Performance from the Nanoscale (CAMP-Nano), State Key Laboratory for Mechanical Behavior of Materials, Xi'an Jiaotong University, Xi'an 710049, China

[c]Department of Nuclear Science and Engineering and Department of Materials Science and Engineering, Massachusetts Institute of Technology, Cambridge, Massachusetts 02139, USA. E-mail: liju@mit.edu

[d]Theoretical Division, Los Alamos National Laboratory, Los Alamos, New Mexico 87545, USA

† Electronic supplementary information (ESI) available. See DOI: 10.1039/c3nr05258c

then possible for these different levels of martensitic organization to appear (nucleate) at *different* times? If so, *which* stage of the hierarchical martensitic nucleation does the measured plateau stress τ_P correspond to? And how would the sample size D affect the martensite hierarchy and superelasticity?

The cause of the TMT hierarchical superstructure shown in Fig. 1(a) is much appreciated. The length scale λ_1 of level-1 structure alternation such as polysynthetic twin thickness is set by the competition between locally fluctuating elastic strain energy, which prefers fine superstructures, and interfacial energy, which prefers coarse superstructures.[19] Fundamentally the same energy-minimization argument can also be applied to SIMT, including stress-driven deformation twinning (DT) which is a special case of SIMT involving no phase change. For example, recently it has been observed that quasi-periodic nano-twinned superstructures form during DT of small-volume Mg samples,[20] shown in Fig. 1(b). Fig. 1(c) illustrates the conceptual equivalence in energy minimization between SIMT/DT and TMT: the easiest way is to consider a displacement-controlled loading apparatus that demands average shear strain $\varepsilon^{\text{average}} = 0.2$ in a certain region of the sample. The region can either stay untransformed ($\varepsilon = 0$) or transformed ($\varepsilon^{\text{transform}} = 0.6$) by DT or phase transformation. This then requires roughly a 1 : 2 mixture of the transformed : untransformed regions in SIMT, if elastic strain is ignored (the elastic strain is generally $\ll$ transformation strain) and if dislocation plasticity is not active. So there has to be a binary spatial pattern of transformed/untransformed laths in SIMT/DT, just like the binary pattern of body-centered tetragonal variant1/variant2 in the familiar twin-accommodated austenite–martensite TMT of steels.[19] Like in TMT, λ_1 of SIMT will also be determined by the competition between locally fluctuating elastic strain energy and interfacial energy, governed by the 2nd term in Fig. 1(c), with equivalent $\varepsilon^{\text{variant1}} = -\varepsilon^{\text{average}}$ and $\varepsilon^{\text{variant2}} = \varepsilon^{\text{transform}} - \varepsilon^{\text{average}}$, and mixing weight w of the two "variants" just like twin-accommodated TMT of steels. Although the number of phase-transformed (level-1) variants after SIMT may differ from that after TMT, and the anisotropy of stress may favor just a single variant (mixed with untransformed austenite), the existence of such a energy-minimizing level-2 superstructure in SIMT/DT means that the nucleation of martensite may be a highly cooperative process across a length scale of at least several λ_1's.

Recent studies on single crystal SMA pillars have shown that the critical stress for SIMT increases dramatically with decreasing pillar diameter D. However, we also notice an interesting phenomenon: the stress plateau of the stress–strain curve for SIMT disappears with reducing pillar diameter.[8–11] Our own experiment, described below, indicates that (a) τ_P matches with level-2 nucleation but not level-1 nucleation and (b) when the sample size D is smaller than level-2 critical nuclei size L_{2c}, the nucleation hierarchy is interrupted, and as a result, the superelasticity behavior changes qualitatively, where instead of an abrupt stress plateau we obtain a continuously rising stress–strain curve.

Here we carried out *in situ* compression tests to observe SIMT directly by TEM. To exclude the effect of oxidization, we chose CuAlNi instead of TiNi (very easy to be oxidized and the transformation is sensitive to alloying[22]) that were studied previously.[8,9] The starting material is the ingot bulk 81.8Cu–14.2Al–4.0Ni (wt.%) single crystal. It was initially solution treated at 1273 K for 1 h and quenched with ice water. The transformation temperatures from the parent phase (DO_3) to martensite (2H) are $M_s = 306.02$ K, $M_f = 295.09$ K, $A_s = 307.77$ K, and $A_f = 329.26$ K, thus the sample at room temperature is in a low temperature martensite (2H) state. Free-standing pillars were then fabricated from the 2H sample using a dual-beam focused-ion-beam (FIB), with the conditions of 15 kV for the gallium ion-beam and 30 kV for the electron-beam. To minimize the oxide layer and FIB damage by gallium, the current was controlled to be 1.5 pA during the finishing processes. To facilitate characterization of the microstructure evolution by TEM, the pillars were machined to be in a tetragonal shape, the thickness is controlled to be thinner than 150 nm in the incident electron beam direction to facilitate observation.

The *in situ* compression is along the axial direction of the pillars, which deviates from [101] about 5°. The zone axis for TEM imaging is along the [010] direction. Electron diffraction patterns indicated that the pre-deformed pillars remain single-crystalline 2H. The *in situ* compression testing was carried out in a JEOL 2100F FEG TEM with a Hysitron PicoIndenter PI-95 system on the martensitic submicron pillars in displacement-controlled mode due to its greater sensitivity to transient phenomena.[23] The microstructure is recorded with a Gatan 830 CCD camera in real-time.

It is known that the 2H phase in the bulk 81.8Cu–14.2Al–4.0Ni (wt.%) single crystal transforms into the 18R phase upon loading.[24] In the following, we present the size dependence of the stress-induced 2H to 18R phase transformation. We first show the results of *in situ* compression on a large pillar with width $D = 950$ nm, thickness 145 nm, and axial length 1290 nm. Fig. 2(b) shows the dark-field image of the pillar before compression and the corresponding diffraction pattern is shown in the upper-left of Fig. 2(h). We note that neither an oxide layer or implanted Ga layer can be observed in Fig. 2(b), nor the amorphous ring exist in Fig. 2(h), indicating the FIB damage and oxidation in the present sample is much less than TiNi.[9] The loading direction (LD) is along the axis of the pillar. We note typical superelastic behavior upon loading and unloading (Fig. 2(a)); the stress–strain curve exhibits a pronounced flat stress plateau upon loading, and there is no permanent crystal structure change after complete unloading (from the corresponding diffraction pattern shown in the upper-left and bottom-right of Fig. 2(h), respectively). Such behavior is consistent with the classical theory of superelasticity by SIMT in bulk.[1,24,25] To check whether the substrate deformation plays a role in the stress–strain curve, we calculated the strain of the pillar according to the height change in its TEM image and compared it with the stress–strain curve in Fig. 2(a) where the total strain is 4.65%. As show in Fig. 2(b) and (f), the maximum strain of the pillar obtained from the micrographs is $(1290–1229)/1290 = 0.0472$, which is consistent with the maximum strain (point f, 0.0465) in the stress–strain curve; in addition, the length of deformed (Fig. 2(g)) and undeformed pillars (Fig. 2(b)) is almost the same. All these

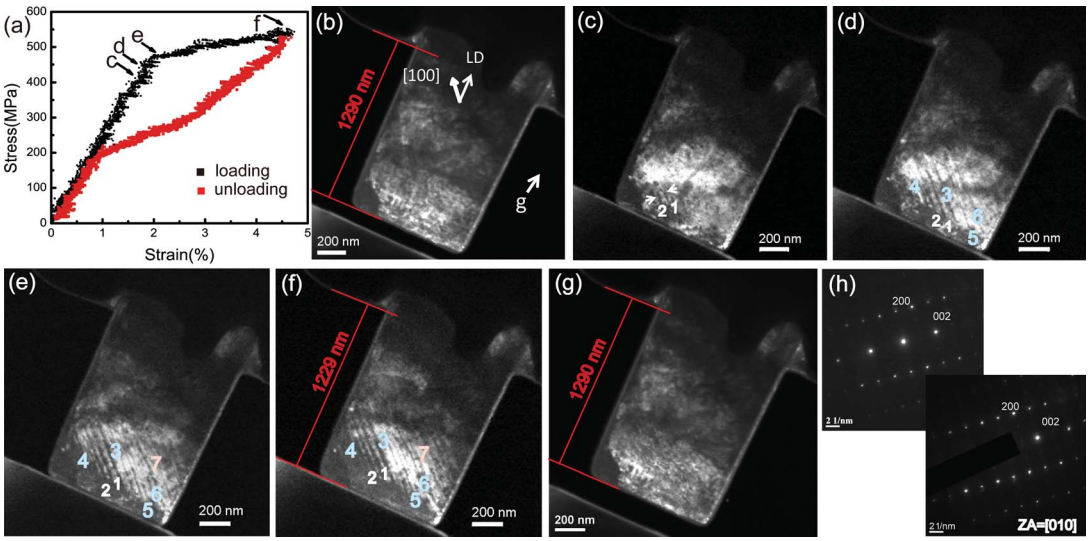

Fig. 2 *In situ* compression of a large pillar with 950 nm width, 145 nm thickness and 1290 nm axial direction. The martensite organization of the pre-mature level-2 nucleus has been formed prior to the onset of the transformation plateau. (a) Strain–stress curve shows typical superplastic behavior. (b) Dark-field image *before* compression (LD is the loading direction). (c–e) Dark-field images corresponding to the points marked in (a). (f) Micrograph at the largest strain of point f. (g) Dark-field image after removing the loading. (h) Diffraction patterns before (upper left) and after compression returned to the original state (bottom right) showing that the crystal structure does not change *before* and *after* compression. All dark-field images are shown in a $g = [202]$ condition and zone axis ZA = [010]. The number of 1–7 in (d), (e) and (f) labels the sequence of generated martensite laths upon loading.

indicate that substrate deformation is a minor factor in the present study.

We note from the dark-field images during the compression that the 18R phase nucleates prior to the onset of the plateau in the stress–strain curve. When the applied strain reaches point c in Fig. 2(a), two 18R phase lamellae (1 and 2, marked by arrows in Fig. 2(c)) have already nucleated and begun to grow. When the stress reaches d, which is just near the onset of the plateau, a large cluster of polysynthetic laths (3–6, marked in Fig. 2(d)) is nearly simultaneously formed and grows to longer than 500 nm instantly. With further loading, the facile growth of the "mature" cluster of polysynthetic laths (1–6) leads to the abrupt occurrence of a stress plateau. In the plateau region, the martensite lamellae grow continuously along the [100] direction as well as widen in the transverse direction. Once the lamellae approach the left side of the pillar as close as about 200 nm, another new martensite lamella (7 in Fig. 2(e)) nucleates from the right side of the pillar and grows rapidly along the same [100] direction (Fig. 2(e)). At the largest strain, shown in Fig. 2(f), the laths grow along both the longitudinal and transversal directions. Compared with Fig. 2(e), the laths, in particular 1, 2 and 3, almost extend to the left side of the pillar, whereas the widened laths 2 and 4 tend to coalesce to one lath. The details for the transformation are shown in Movie S1†. In this way the system transforms smoothly from 2H to 18R in the plateau region. We note that the transformation plateau strain is about 2%, which is consistent with the transformation strain from 2H to 18R in bulk,[1,24] and by lattice correspondence. The level-2 critical nuclei size L_{2c} is thus identified to be around 500 nm, below which the cluster of polysynthetic laths is still energetically subcritical, and thus continuous rise of external stress is required to make the cluster grow. But once $L_2 > L_{2c}$, the level-2 organization becomes energetically favorable to grow unbounded in size at fixed stress, as in bulk samples (see Fig. 4 in ref. 21 for details). It is noted that the hierarchical superstructure with alternative laths in Fig. 2(d) corresponds to the level-2 superstructure, *i.e.* the mixture of transformed 18R and untransformed 2H with the alternation length scale of λ_1 on the order of 30 nm.

We now explore the behavior of SIMT in smaller pillars. A pillar with width $D = 456$ nm, thickness 110 nm and axial length 873 nm (as shown in Fig. 3(b)) was chosen. The loading direction is the same as the large pillar. The obtained strain–stress curve (Fig. 3(a)) shows that the transformation plateau disappeared. To further confirm that the 2H to 18R phase transformation does occur in the smaller pillar, we checked the diffraction pattern during the *in situ* compression and the result is shown in Fig. 3(c). Compared to the diffraction patterns *before and after* compression (inset: upper right and bottom right in Fig. 3(b) respectively), the diffraction pattern under 5% compressive strain (Fig. 3(f)) shows the extra spots of 18R, $(206)_{18R}$, $(20\bar{1}\bar{2})_{18R}$, and $(00\bar{3}\bar{6})_{18R}$, demonstrating a stress-induced 2H to 18R phase transformation in the smaller pillar. In addition, the lack of any difference in the diffraction patterns *before* and *after* compression also suggests that the stress-induced 2H to 18R phase transformation is reversible after unloading.

The corresponding bright-field images during *in situ* compression show that this behavior results from the successive nucleation of 18R laths. Upon compression, two 18R nuclei initially form (1 and 2, shown in Fig. 3(d)) and then extend to 100 nm at point d in Fig. 3(a). When the applied strain reaches

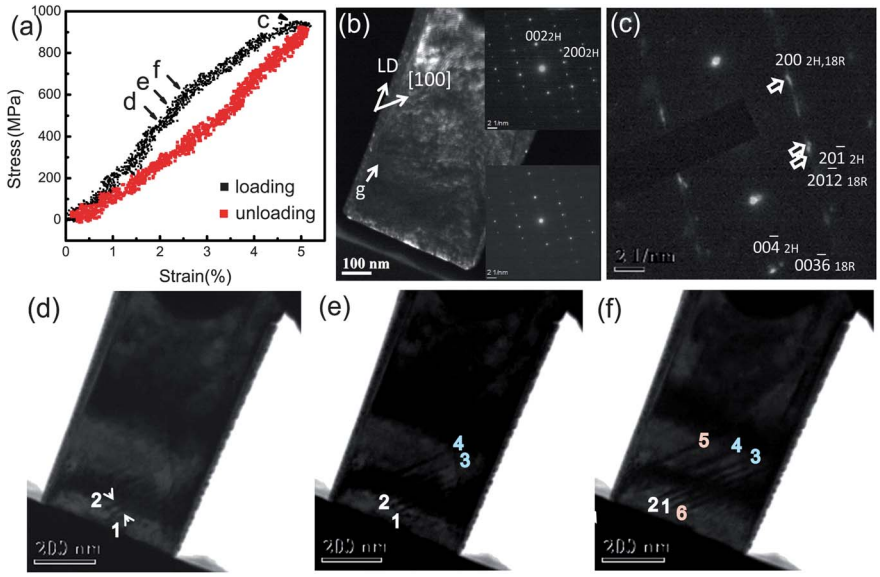

Fig. 3 *In situ* compression of a smaller pillar with width 456 nm, thickness 110 nm and axial direction 873 nm. (a) Strain–stress curve shows the disappearance of the stress plateau. (b) Dark-field image of the pillar and its diffraction patterns *before* and *after* compression (inset: upper right and bottom right, LD is the loading direction). (c) Diffraction pattern at a strain near 5% (as indicated by arrow c in (a)) and zone axis ZA = [010]. (d), (e) and (f) are bright-field images of the pillar at marked points d, e and f in (a), numbers 1–6 in (d), (e) and (f) label the sequence of generated martensite laths upon loading.

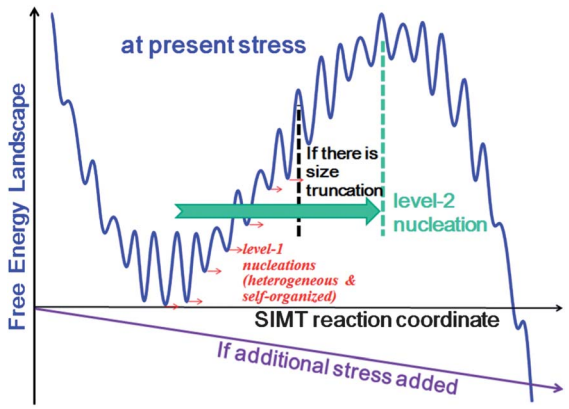

Fig. 4 Schematic energy landscape for hierarchical nucleation, where the reaction coordinate is defined along a tortuous, "pipe-like" path in microscopic state space, reflecting heterogeneity and cooperativity in the material system undergoing stress-induced martensitic transformation (SIMT). The blue curve shows the free energy landscape at the present stress, some level-1 transformations have already occurred due to the surface and residual stress heterogeneities. The system will stay at this state if no additional stress is applied. If "additional stress is added" (the purple curve), the present state would no longer be stable and the system would be propelled further. Once the level-2 hump is overcome, the level-1 embryos would run wild and occupy the entire sample. However, size truncation will interrupt the level-2 nuclei formation if the sample is smaller than the level-2 critical nuclei size.

point e in Fig. 3(a), another two nuclei (3 and 4 in Fig. 3(e)) generate and grow with the applied stress. At even higher strain (point f in Fig. 3(a)), other newly formed martensite plates (5 and 6 as shown in Fig. 3(f)) are also seen.

However, in contrast to that in large pillars, the transformation here is dominated by sequential level-1 nucleations of 18R during the whole loading. A sharp nucleation point of the level-2 superstructure cannot be identified, because the 18R laths run out of the sample before reaching the critical size L_{2c}; the "pre-mature" cluster of polysynthetic laths requires stress increase to grow. As a result, the stress in the curve of the smaller pillar continuously increases over the whole range of transformation, and the superelasticity plateau disappears (see Movie S2† for details).

The experimental results above show that careful parsing of the term "martensite nucleation" is required, because the word "martensite" is a polyseme that can either mean the transformed crystal structure (level-1) or the various higher-order superstructures that one sees in metallographic characterizations. In compressing the bigger sample, we observed a very clear diffraction pattern of 18R long before τ_P was reached; concomitantly, in the imaging mode we saw individual 18R laths extending hundreds of nanometers. Thus, level-1 nucleation must have occurred before τ_P. Such phase transformation should be heterogeneous, as we saw the laths started from the surface (Fig. 2(c)). In addition, as level-1 nucleation corresponds to atomic lattice shear and its embryo is only a few atomic layers thick, the critical level-1 nuclei size L_{1c} is below the spatial–temporal resolution (>4 nm, 30 frames per s) of the present *in situ* TEM technique, and so we cannot characterize these heterogeneous nucleations with any reasonable descriptor experimentally.

The level-2 nuclei size L_{2c}, however, appears to be ~500 nm, well within the resolution of *in situ* TEM. With the level-2 SIMT nucleus captured by TEM in Fig. 2(d) and (e), the remaining task is to rationalize L_{2c} theoretically. The origin of such an L_{2c} was already hinted in previous theoretical studies of deformation twinning and martensite nucleation.[20,26–29] A common feature of

the numerical simulation results is that the computed minimum energy path (MEP) based on which the reaction coordinate is defined takes a "tortuous pipe"-like path to minimize the energy, which is not a straight bee-line connecting the initial (untransformed) with the final SIMT state in configurational space, that is, the critical level-2 nuclei can look very different from the final product in terms of variant volume fraction and also shape.[29] The exact MEP of level-2 nucleation for a set-up like our *in situ* contact experiment would depend on the applied and residual stress distributions, and pre-existing microstructures such as surface conditions, and can be rather complex. But generically, the critical length scale L_{2c} for a self-organized superstructure ("strain superlattice" or "strain crystal" as shown in Fig. 1(c) and (b),[20] and 2(d)) to nucleate in an infinite body arises from the external work plus self-elastic energy and competition with interfacial energy. Generally speaking, the work plus residual energy E_{elastic} after self-organization still has different size scaling with the interfacial energy E_{int} (interfaces between 2H/18R and between different-18R laths), thus giving rise to L_{2c}. The size of such a "strain crystal" nucleus L_{2c} should encompass at least several λ_1's, or "strain periods", even for very high stresses, just as atomic crystal nucleus L_{1c} should encompass at least several atomic lattice spacings. If the sample size D is smaller than L_{2c}, then the nucleation hierarchy is interrupted. With $D < L_{2c}$, the measured mechanical response will result from the "pre-mature" part (before the dashed line) of the energy landscape shown in Fig. 4. The details of this "pre-mature" self-organization will thus dominate the mechanical response of the small-volume, size-confined SMAs, such as wires, pillars and particles.[6,18,30] This is qualitatively different from that of bulk samples, where details of the "pre-mature" landscape are not as important for the bulk mechanical behavior.

Another aspect of this work is that we do not find relatively larger energy dissipation in the smaller-sized Cu–14.2Al–4.0Ni SMA pillar, as is the case reported in ref. 11. Comparing our Fig. 3(a) with 2(a), the smaller pillar shows clear size strengthening. But the loss factor $\eta \equiv \Delta W/\pi W_{\max}$, where ΔW is the dissipated energy per stress–release cycle and $W_{\max}$ is the maximum stored energy per unit volume over the cycle,[11] is somewhat smaller for the smaller pillar (0.064) than that for the larger pillar (0.076). The reason for this discrepancy in experimental results is not clear. But, theoretically speaking, overcoming the nucleation barrier in finite time is a mechanistic origin for dissipation; so if only level-1 nucleation occurs, and level-2, 3, … nucleations are avoided, then perhaps the reduction in dissipation for the smaller pillar can be rationalized. Also, the quite long aspect ratio of our TEM compression specimens may introduce some bending artifact, but if so our larger specimen (aspect ratio 8.9) should produce more severe bending artifact than our smaller specimen (aspect ratio 7.9), while Fig. 2(a) agrees quite well with bulk response.

In summary, we directly observed the hierarchical nucleation of martensitic transformation and find that the onset of the stress plateau in the stress–strain curve corresponds to level-2 nucleation rather than level-1 nucleation. However, when the sample size D is smaller than the level-2 critical nuclei size ($L_{2c} \sim 500$ nm), the nucleation hierarchy is interrupted, the low-level "pre-mature" nuclei dominate the mechanical response (superelasticity). As the premature nuclei are still energetically subcritical and require stress increase to grow before reaching the critical size L_{2c}, the stress continuously increases over the whole range of transformation. Thus, the superelasticity plateau disappears. The present work provides an essential piece of information for adopting shape memory alloys in miniaturized MEMS/NEMS devices, as well as a conceptual basis for understanding the observed phenomena.

Acknowledgements

This work was supported by 973 Programs of China (2010CB631003, 2012CB619402) and NSFC (51171140, 51231008, 51320105014 and 51321003), as well as 111 Project of China (B06025). JL acknowledges support from NSF DMR-1240933 and DMR-1120901. The authors would like to thank Professor Zhiwei Shan and Evan Ma for helpful discussion of some of the results presented in this paper.

Notes and references

1 K. Otsuka and C. M. Wayman, *Shape memory materials*, Cambridge University, Cambrige, UK, 1998.
2 W. M. Huang, Z. Ding, C. C. Wang, J. Wei, Y. Zhao and H. Purnawali, *Mater. Today*, 2010, **13**, 54–61.
3 E. Patoor, D. C. Lagoudas, P. B. Entchev, L. C. Brinson and X. J. Gao, *Mech. Mater.*, 2006, **38**, 391–429.
4 K. Bhattacharya, S. Conti, G. Zanzotto and J. Zimmer, *Nature*, 2004, **428**, 55–59.
5 D. C. Lagoudas, *Shape Memory Alloys: Modeling and Engineering Applications*, Springer-Verlag US, Boston, MA, 2008.
6 K. Bhattacharya and R. D. James, *Science*, 2005, **307**, 53–54.
7 M. Y. Razzaq, M. Behl and A. Lendlein, *Nanoscale*, 2012, **4**, 6181–6195.
8 C. P. Frick, S. Orso and E. Arzt, *Acta Mater.*, 2007, **55**, 3845–3855.
9 J. Ye, R. K. Mishra, A. R. Pelton and A. M. Minor, *Acta Mater.*, 2010, **58**, 490–498.
10 Y. Chen and C. A. Schuh, *Acta Mater.*, 2011, **59**, 537–553.
11 J. San Juan, M. L. No and C. A. Schuh, *Nat. Nanotechnol.*, 2009, **4**, 415–419.
12 D. C. Dunand and P. Müellner, *Adv. Mater.*, 2011, **23**, 216–232.
13 Y. Chen, X. Zhang, D. C. Dunand and C. A. Schuh, *Appl. Phys. Lett.*, 2009, 95.
14 J. San Juan, M. L. Nó and C. A. Schuh, *Adv. Mater.*, 2008, **20**, 272–278.
15 A. Ibarra, J. San Juan, E. H. Bocanegra and M. L. Nó, *Acta Mater.*, 2007, **55**, 4789–4798.
16 T. Ezaz, H. Sehitoglu and H. J. Maier, *Acta Mater.*, 2011, **59**, 5893–5904.
17 K. M. Liew and J. J. Zhu, *Mech. Adv. Mater. Struct.*, 2004, **11**, 227–248.
18 T. Waitz, K. Tsuchiya, T. Antretter and F. D. Fischer, *MRS Bull.*, 2009, **34**, 814–821.

19 M. S. Wechsler, D. S. Lieberman and T. A. Read, *Trans. Am. Inst. Min. Metall. Eng.*, 1953, **197**, 1503–1515.
20 Q. Yu, L. Qi, K. Chen, R. K. Mishra, J. Li and A. M. Minor, *Nano Lett.*, 2012, **12**, 887–892.
21 D. Z. Liu and D. Dunne, *Scr. Mater.*, 2003, **48**, 1611–1616.
22 J. Zhang, G. Fan, Y. Zhou, X. Ding, K. Otsuka, K. Nakamura, J. Sun and X. Ren, *Acta Mater.*, 2007, **55**, 2897–2905.
23 A. M. Minor, S. A. Syed Asif, Z. Shan, E. A. Stach, E. Cyrankowski, T. J. Wyrobek and O. L. Warren, *Nat. Mater.*, 2006, **5**, 697–702.
24 K. Otsuka, H. Sakamoto and K. Shimizu, *Acta Metall.*, 1979, **27**, 585–601.
25 B. Kockar, I. Karaman, J. I. Kim, Y. J. Chumlyakov, J. Sharp and C. J. Yu, *Acta Mater.*, 2008, **56**, 3630–3646.
26 S. Ogata, J. Li and S. Yip, *Phys. Rev. B: Condens. Matter Mater. Phys.*, 2005, **71**, 224102.
27 M. L. Nó, A. Ibarra, D. Caillard and J. San Juan, *Acta Mater.*, 2010, **58**, 6181–6193.
28 A. Ibarra, J. San Juan, E. H. Bocanegra, D. Caillard and M. L. Nó, *Mater. Sci. Eng., A*, 2006, **438–440**, 787–790.
29 C. Shen, J. Li and Y. Z. Wang, *Metall. Mater. Trans. A*, 2008, **39**, 976.
30 T. Waitz, D. Spisak, J. Hafner and H. P. Karnthaler, *Europhys. Lett.*, 2005, **71**, 98–103.

